# CrystEngComm

Accepted Manuscript

ROYAL SOCIETY OF CHEMISTRY

www.rsc.org/crystengcomm

Journal Name

ARTICLE

# Polyanionic Identity Of $Ca_2Zn_2(V_3O_{10})(VO_4)$ Photocatalyst Manifested by X-ray Powder Diffraction And Periodic Boundary Density Functional Theory Calculations

Received 00th January 20xx,
Accepted 00th January 20xx

DOI: 10.1039/x0xx00000x

**www.rsc.org/**

Artem A. Babaryk,[a,b] Ievgen V. Odynets,[a] Sergei Khainakov,[b] Santiago Garcia-Granda,[b] Nikolay S. Slobodyanik[a]

The structure of photocatalytic and photoluminiscent binary vanadate of general formula “$CaZnV_2O_7$” has been investigated using X-ray powder diffraction. The compound is built up of isolated $[V_3O_{10}]$ and $[VO_4]$ being this complex trivanadate-vanadate, in opposition to previous suggestions on isostructurality “Ca*M*$V_2O_7$”, M – Mg or Co (Murashova *et al.*, 1991, 36, 617-621).The present model has been confirmed by theoretical calculations. Thermal analysis and scanning electron microscopy have been performed and the electronic structure analysis has been found in an agreement with reference to experimental observations.

## Introduction

Solar cell technology is considered to be a headmost solution for a new “green society” era which is called for the replacement of traditional fossil fuel. It is based on the idea of harvesting of solar energy to be absorbed by efficiently and converted into a photocurrent with a dedicated material. Metal oxide semiconductors provide a vast research field to tailor solar absorbing materials employing the so-called band gap design approach[1]. In particular, it has been shown that, the $V^{5+}$-containing oxides could absorb UV to visible light invoking charge transfer (CT) transitions. So far, the ortho-, pyro- and polyvanadates: $AVO_4$ (*A*=Fe, Y, Ce, Nd, Sm, In, Bi)[2-6], $LiNiVO_4$[7], $Bi_4V_2O_{11}$[8], $A_3V_2O_8$ (*A* = Mg, Ni, Zn, Cu)[9,10], $BiZn_2VO_6$[11], $Ag_3VO_4$[12], $Mn_2V_2O_7$[13], $ZrV_2O_7$[14],$Ag_4V_2O_7$[15], $Fe_2V_4O_{13}$[16], $Na_2V_6O_{11}\cdot xH_2O$[17] have been proven to demonstrate the visible-light induced photo-catalytic activity without competing with chemical stability. The 3d-orbitals of vanadium can lower the conduction band energies compared to the analogous titanates, niobates, and tantalates[1]. The mixed-metal vanadium oxides have shown great potential in photocatalytic reactions.

Recently, Wang et al.[18] has been demonstrated “$CaZnV_2O_7$” was a visible-light-driven photocatalyst active in photodegradation of methylene blue dye as a model water pollutant. In addition, upon doping of it with $Yb^{3+}$, effective ultraviolet-to-nearinfrared light conversion is achieved with

---

[a] *Faculty of Chemistry, Taras Shevchenko National University of Kyiv, Volodymyrska 64/13, 01601 Kyiv, Ukraine*
[b] *2Department of Physical and Analytical Chemistry, Faculty of Chemistry, University of Oviedo-CINN, C/ Julian Claveria 8, 33006 Oviedo, Spain*

† Footnotes relating to the title and/or authors should appear here.
Electronic Supplementary Information (ESI) available: [details of any supplementary information available should be included here]. See DOI: 10.1039/x0xx00000x

quantum efficiency of 18.5% at 5% doping level[19]. While knowledge on a structural organization is of high importance to deep understanding of physical properties, hitherto "$CaZnV_2O_7$" has not been characterized properly. Data mining on the reference is given to JSPDS card #00-036-0170 is marked as "low-precision" quality and does not contain any structural information. According to Murashov et al.[20], the compound under interest is isostructural to $CaMgV_2O_7$, contains $[V_4O_{14}]$ tetravadate moieties. Hence, proper attribution of "$CaZnV_2O_7$" to distinct class of polyvanadates using X-ray powder diffraction and periodic boundary density functional theory is the subject of present study.

## Experimental

### Synthesis

The polycrystalline powder of $CaZnV_2O_7$ was synthesized by conventional solid-state reaction techniques. The mixtures of $CaCO_3$, ZnO and $NH_4VO_3$ (all reagents have p.a. grade) at a molar ratio 1:1:2 was milled in an agate mortar for half hour. Synthesis of compound was carried out at ceramic crucible. After an initial heat treatment at 350 °C for 6 h, sample was calcined at an optimized temperature (700 °C) for 20 h. The mixture was re-ground between heating and pressed (P = 105 N $m^{-2}$) into the pellet (Ø = 20 mm, d = 2 mm).

### X-ray powder diffraction

The pattern was collected at room temperature on a PanalyticalX'Pert Pro diffractometer, equipped with a one-dimensional hybrid pixel technology position sensitive device detector (PIXcel™) and operating with Ni-filtered CuKα radiation. Structural refinements were developed from the powder pattern using Rietveld analysis[21](Figure 1). Initial atomic coordinates were taken from ref. [16].Forisotypical structure. Scale factor, Chebyshev polynomials up to 20-th order, cell parameters, fractional atomic coordinates, its isotropic displacement parameters (IDPs) and Lorentzian size/strain contributions according to Balzar's (Double Voight) approach[22]were used to model sample function. Instrumental function was deconvoluted by fundamental parameters approach[23], implying physical constants of the diffractometer and apertures of optical components to be known. Preferred orientation of crystallites was modelled by spherical harmonics series expanded to 4-th order independent terms for 2/m symmetry class. For oxygen, calcium, vanadium and zinc atoms IDPs were refined in groups segregated upon the atomic scattering factor. Bond valence sum [$BVS = \exp(R\text{-}Ro/b)$] restrains were used as a penalty function for V-O and Zn-O interatomic distances[24]. Relative amounts of trace phases were estimated by PONKS method[25] due to undetermined structure of it. Relevant phase information and final coordinates are summarized in Tables 1,2.

(Figure 1 shoud be here)

Figure 1. Rietveld analysis plot of $Ca_2Zn_2(V_3O_{10})(VO_4)$ X-ray powder diffraction pattern ($Y_{obs}$, $Y_{calc}$ and $Y_{obs}$-$Y_{calc}$ are drawn as a blue, red and grey solid lines, Bragg peak positions of the main phase and traces are shown as blue, green and black tickmarks).

Table 1. A summary of crystal data, data acquisition and structural refinements.

| | |
|---|---|
| Diffractometer | PanalyticalX'Pert Pro |
| Radiation | CuKα, $\lambda$ = 1.5418 Å ($Ni_\beta$-filter) |
| Temperature | 291(2)K |
| Step size | 0.013° |
| Composition, formula weight | $Ca_2Zn_2V_4O_{14}$, 638.68 |
| Space group, Z | $P2_1/c$, 4 |
| Unit cell parameters | $a$=6.8093(2), $b$=14.5094(3),<br>c=11.2568(3), $\beta$=99.471(2)° |
| Number of reflections | 3480 |
| $R_p$, $R_{wp}$, $\chi^2$ | 0.014, 0.019, 1.145 |

Table 2. Fractional atomic coordinates and isotropic displacement parameters (Å$^2$).

| Atom | $x$ | $y$ | $z$ | $B_{iso}$ |
|---|---|---|---|---|
| Zn1 | −0.0125(9) | 0.2529(4) | 0.2515(5) | 3.31(17) |
| Zn2 | 0.3533(8) | 0.1743(3) | 0.4269(4) | 3.31(17) |
| Ca1 | 0.6703(11) | 0.1225(6) | 0.0201(6) | 2.9(2) |
| Ca2 | 0.9468(11) | 0.0067(7) | 0.7529(7) | 2.9(2) |
| V1 | 0.4880(8) | 0.2037(3) | 0.7089(3) | 2.21(14) |
| V2 | 0.4091(9) | 0.0157(3) | 0.6829(5) | 2.21(14) |
| V3 | 0.1466(8) | −0.13833(17) | 0.5173(3) | 2.21(14) |
| O1 | 0.5839(8) | 0.0889(3) | 0.7664(8) | 1.89(17) |
| O2 | 0.2574(9) | 0.2480(10) | 0.7310(15) | 1.89(17) |
| O4 | 0.6516 (9) | 0.2840(4) | 0.6960(16) | 1.89(17) |
| O5 | 0.410(2) | 0.1383(4) | 0.5885(4) | 1.89(17) |
| O6 | 0.6401(16) | −0.0420(9) | 0.6934(16) | 1.89(17) |
| O7 | 0.2370(19) | −0.0302(4) | 0.5351(8) | 1.89(17) |
| O8 | 0.2930(9) | −0.0155(12) | 0.7896(7) | 1.89(17) |
| O9 | −0.0377(14) | −0.1420(11) | 0.6089(6) | 1.89(17) |
| O10 | 0.068(2) | −0.1372(10) | 0.3798(4) | 1.89(17) |
| O11 | 0.3881(12) | −0.2253(9) | 0.5638(19) | 1.89(17) |
| O3 | 0.3620(8) | 0.3209(4) | 0.5456(13) | 1.89(17) |
| V4 | 0.1572(3) | 0.3740(4) | 0.5182(4) | 2.21(14) |
| O12 | 0.037(2) | 0.3650(15) | 0.3732(4) | 1.89(17) |
| O13 | −0.0077(12) | 0.3575(14) | 0.6335(6) | 1.89(17) |
| O14 | 0.236(3) | 0.4918(5) | 0.5111(17) | 1.89(17) |

### Chemical Composition and Microstructure

Scanning electron microscopy (SEM) images (Figure S1, S2) were recorded at 20 kV accelerating voltage with a JEOL-6610LV scanning electron microscope equipped with Oxford X-Max microanalysis system (EDX), which was used to confirm the composition (Tables S3).

### Thermal analysis

The thermal behavior of $Ca_2Zn_2(V_3O_{10})(VO_4)$ batch was studied on a simultaneous thermogravimetry/differential thermal analyzer Shimadzu DTG-60H. The sample and reference ($Al_2O_3$) were enclosed in Pt/Rh crucibles, heated from room temperature to 800 °C under air atmosphere (flow 100 ml $min^{-1}$) at a rate of 10° $min^{-1}$.

### Computational aspects

Periodic boundary density functional calculations were performed with DMol3 package[26]. The calculations were performed with "double-numeric plus polarization" (DNP) basis set. Generalized gradient approximation (GGA) based on the Perdew-Burke-Enzernhof formalism[27] was applied for exchange–correlation functional. Real-space global cut-off radii were set for all elements at 6.1 Å to insure accurate numerical integration for orbitals. Brillouin zone sampling was carried out by choosing a Monkhorst-Pack grid with spacing of 0.05 $Å^{-1}$ between k-points. Calculated total energy differs only by $10^{-5}$eV/atom when choosing a denser grid or larger cut-off radii implying that the results were well converged. The geometry optimization convergence thresholds for energy and Cartesian components of internal forces were set to be $10^{-5}$eV/atom and 0.005 eV $Å^{-1}$ respectively.

## Results and discussion

### Thermoanalytical study

TG and DTA curves of $Ca_2Zn_2(V_3O_{10})(VO_4)$ batch is shown on the Figure 2. The chemical transformations of initial mixture are accompanied with weight losses due to the stepwise decomposition with elimination of volatile products.

The first weight loss on the TG curve occurs in temperature range from 170 to 330 °C with two endothermic (192 and 233 °C) and one exothermic (315 °C) sharp peaks. It is attributed to thermal decomposition of $NH_4VO_3$ molecules with disengagement of the ammonia and water molecules. Experimental data (12.88 wt. %) are in a good agreement with calculated difference of mass (12.53 wt. %). The second phase of the thermal decomposition is caused by destruction of $CaCO_3$withan its onset ca. 590 °C reaching the maxima at 609 °C (endothermic effect). The completion of $CO_2$removal is detected at 700 °C(observed weight loss – 10.83% wt.).

(Figure 2 shoud be here)

Figure. 2. TG/DTA trace for the reacting mixture.

At the temperature of 707 °C, the exothermic effect occurs which is attributed to the formation of the target compound. The very last endothermic peak is observed on the DTA curve at 735 °C ascribed to the fusion of $Ca_2Zn_2(V_3O_{10})(VO_4)$.

### Crystallographic description

Asymmetric unit cell contains 22 atoms: all of them located at general positions of 4e Wyckoff site symmetry. V1 and V2 are being in 4-, 5-fold oxygen environment and sharingO1 and O5 bridging atoms are serving as a common edge of bisphenoidal $[V1O_4]$ and square pyramidal $[V2O_5]$ coordination polyhedra. $[V3O_4]$ tetrahedron completes anionic moiety augmenting it via terminal O7 apex into a $[V_3O_{10}]$ group. Velikodnyi et al. suggested a presence of $[V_4O_{14}]$ anionic groups for $SrMgV_2O_7$[28], $SrPbV_2O_7$, $PbMgV_2O_7$ and $PbZnV_2O_7$[29], $CaMgV_2O_7$ and $CaCoV_2O_7$[16]. An inspection of a cross-section of calculated static deformation density where V2, V3 and V4 atoms were mapped, displays the absence of any noticeable interaction between terminal O3 and V1 atom (Figure 3): accumulated electron density around O3 is distributed symmetrically opposed to outspread regions in vicinity of shared O1, O5 and O7 atoms.

(Figure 3 shoud be here)

Figure 3. Calculated best-plane iso-section ($\Delta\rho$ = 0.05 e $Å^{-3}$) of static deformation electronic density (scale maximum and minimum are set to 0.351 e $Å^{-3}$ and -0.515 e $Å^{-3}$).

This result confirmed by CHARDI calculations[30] for which returned $Q$(O3) effective charge within V4 sphere of enclosure is virtually null. As the third criteria an empirical comparison of V…V separations can be used for closely related compounds the genuine tetravanadates $GaZn_2V_3O_{11}$[31], $FeMg_2V_3O_{11}$ and $FeZn_2V_3O_{11}$[32] are considered in the case where the sequence $V_{tetr}\cdots V_{bpy}\cdots V_{bpyr}\cdots V_{tetr}$ (where $V_{bpyr}$ and $V_{tetr}$ denote bypyramidal and (pseudo)tetrahedral coordinated V atoms)takes place likewise for present case. The distances $V_{bpyr}\cdots V_{bpyr}$ and $V_{bpyr}\cdots V_{tetr}$ are near 2.98 and 3.45 Å. Table 3 lists calculates interatomic separations for the entire series of isotypical compounds. For target compound, subsequent $V_{tetr}\cdots V_{bpyr}\cdots V_{tetr}$ are found to be 2.82Å and 3.23Å indicate typical values for polyvadate with coordinated vanadium atoms. The terminal contact V3···V4 ($V_{bpyr}\cdots V_{tet}$) is 3.67 Å which is in a contrast with expected averaged value.

**Table 3.** V…V contact distances and calculated charge distribution for $A_2B_2(V_3O_{10})(VO_4)$ compounds.

| Compound* | $V_{bpyr}…V_{bpyr}$ | $V_{bpyr}…V_{tetr}$ | $Q$(V1) | $Q$(V2) | $Q$(V3) | $Q$(V4) | Reference |
|---|---|---|---|---|---|---|---|
| $Ca_2Mg_2(V_3O_{10})(VO_4)$ | 2.803(3) | 3.288(2) | 4.942 | 4.664 | 5.302 | 5.187 | [16] |
| $Ca_2Co_2(V_3O_{10})(VO_4)$ | 2.813(3) | 3.278(2) | 4.939 | 4.646 | 5.269 | 5.219 | [16] |
| $Ca_2Zn_2(V_3O_{10})(VO_4)$ | 2.824(1) | 3.232(1) | 4.758 | 4.758 | 4.625 | 4.941 | present work |
| $Sr_2Mg_2(V_3O_{10})(VO_4)$ | 2.840(3) | 3.269(3) | 4.980 | 4.583 | 5.292 | -** | [17] |
| $Pb_2Mg_2(V_3O_{10})(VO_4)$ | 3.103(5) | 3.157(5) | 4.883 | 4.993 | 5.135 | 5.037 | [18] |
| $Pb_2Zn_2(V_3O_{10})(VO_4)$ | 2.857(7) | 3.302(6) | 5.280 | 4.744 | 4.592 | 5.623 | [18]] |

*Notes*: *chemical formulas are given uniformly in a line with reported compound while in reference works it appears as $ABV_2O_7$ **coordinates of V4 atoms have not been determined.

Zinc atoms are assembled into edge-sharing $[Zn_2O_{10}]$ bioctadera decorated with eight $[VO_4]$ groups in the second sphere of enclosure: Zn1 central atom adopts O4, O10 and O13 ligands from $[V1O_4]$, $[V3O_4]$ and $[V4O_4]$ residues and Zn2 does the same for O5, O6 and O11 which belongs to $[V2V3O_7]$ and $[V1V2O_7]$. Six-fold environment for zinc atoms is accomplished by bi-dentate capping of $[V4O_4]$ anionic group (Figure 3a).Complete adjacent moieties are bound of each other with $[V3O_4]$ giving rise to infinite ribbons those are running parallel to two-fold axis and shifted for $c$/2 (Figure 3b). The spatial voids in the anionic sublattice host Ca atoms of two distinct kinds. Formally, the first is described as a distorted dodecahedron [2.40<d(Ca1…O)<3.11 Å] and, the second does as a monocapped trigonal prism [2.41<d(Ca2…O)<2.82 Å, but the additional binding via common O8…O13 edge affords bi-centered body. The later continuously propagate along [001] direction in a helical fashion.

(Figure 4 shoud be here)

Figure 4. A view of $[Zn_2(V_3O_{10})(VO_4)]^{-4}$ anionic moiety (top left), a packing of it into chain motif propagating along [001] direction (top right) and oxygen bi-centered polyhedron of Ca1 and Ca2 (bottom left) and its helical structuring collinear to [100] direction through edge-sharing (bottom right).

### Electronic structure analysis

A plot of calculated band structure is presented on Figure 5a. The direct allowed transition $B_v \rightarrow B_c$ occurs at energy of 2.27 eV derived theoretically that is in excellent agreement with experimental value of 2.36 eV for the pristine bulk sample[18]. To explore bonding situation, the total and partial (both atomic and orbital resolved) density of states was examined (Figure 5b). Occupied O2p states dominate from E-Ef=-3.4…0eV.

(Figure 5 should be here)

Figure 4. A diagram of calculated band structure (left) and total, angular momentum and atomically resolved density of states (right).

(at the top valence band) while filled V3d orbitals mostly overlapped the latter within E-Ef=-4.5…-2.5 eV. The higher energy empty V3d orbitals contribute significantly to conduction band. As above, we have confirmed here the compound is polyanionic consists of $(V_3O_{10})^{5-}$ and $(VO_4)^{3-}$. Examining atomic resolved V3d states one can conclude those relative contributions to conduction bands are larger for terminal V3 and V4 atoms. Zn3*d*are found mostly at the bottom of valence states spanning over E-Ef=-6…-4.5 eV range and poorly donate to conduction band. To our knowledge, such peculiarity has been reported for $Zn_3MV_2O_8$ (*M* – V[9]; Nb, Ta[33]) so far. Wang et al.[9] suggested that weak hybridization of Zn3*d* and O2*p* does not affect the band gap, but increases the valence bandwidth resulting in higher hole mobility across it, and therefore, facilitated production of photogenerated $O_2$. Finally, this hypothesis is in good agreement with photocatalytic properties of $Ca_2Zn_2(V_3O_{10})(VO_4)$ demonstrated by the pseudo-first order reaction of degradation of methylene blue model water pollutant under visible light irradiation with $k$=0.00633min$^{-1}$[18].

## Conclusions

Herewith structure and bonding for $Ca_2Zn_2(V_3O_{10})(VO_4)$ was re-estimated involving both X-ray diffraction and DFT theoretical evaluations. It has been shown that the series of isotypical "$ABV_2O_7$" compounds do not belong to a divanadate array. Calculated electronic structure supports recently observed photocatalytic properties of the solid.

## Acknowledgements

Financial support from Spanish Ministerio de Economía y Competitividad (MAT2013-40950-R), Gobierno del Principado de Asturias (GRUPIN14-060) and FEDER funding is acknowledged by AAB, SK and SGG. AAB and IVO acknowledge the JSPDS ICDD Grant-in-Aid program (12-02).

## Notes and references

1 A. Kudo, Y. Miseki, Chem. Soc. Rev., 2009, 38, 253.
2 M. Wang, L.-A. Wang, W.-J. Zhang, L. Bao, L.-L. Yang, Gongneng Cailiao (Journal of Functional Materials), 2009, 40, 201.
3 H. Xu, H. Wang, H. Yan, J. Hazardous Mater.,2007,144, 82.
4 S. Mahapatra, S.K. Nayak, G. Madras, T.N. Guru Row, Ind. Eng. Chem. Res., 2008, 47,6509.
5 J. Xu, C. Hu, G. Liu, H. Liu, G. Du, Y. Zhang, J. Alloys Compd., 2011, 509, 7968.
6 M. Oshikiri, M. Boero, J. Ye, Z.Zou, G. Kido, J. Chem.Phys., 2002, 117, 7313.
7 X. Qiao, Y. Huang, H.J. Seo, Appl. Surf. Sci. ,2014, 321, 488.
8 V. Thakral, S. Uma, Mater. Res. Bull., 2010, 45, 1250.
9 D. Wang, J. Tang, Z. Zou, J. Ye, Chem. Mater., 2005, 17, 5177.
10 S. Zhang, Y. Sun, C. Li, L. Ci, Solid State Sci., 2013, 25, 15.
11 H. Liu, R. Nakamura, Y. Nakato, Electrochem. Solid State Lett., 2006, 9, G187.
12 X. Hu, C. Hu, J. Solid State Chem.,2007, 180, 725.
13 Q. Yan, G. Li, P.F. Newhouse, J. Yu, K.A. Persson, J.M. Gregoire, J.B. Neaton, Adv. Energy Mater., 2015, 1401840.
14 P.P. Sahoo, S. Sumithra, G. Madras, T.N. Guru Row, Inorg. Chem., 2011, 50, 8774.
15 K. Kuribayashi, E.Nozawa, Y. Iyama, H. Hirai, S. Namba, T. Kugita, (2008) A Global Road Map for Ceramic Materials and Technologies: Forecasting the Future of Ceramics, International Ceramic Federation - 2nd International Congress on Ceramics, ICC 2008, Final Programme, 5 p.
16 Y.-Y. Zhang, C. He, J.-H. Deng, Y.-T. Tu, J.-K. Liu, Y. Xiong, Res. Chem. Intermediates, 2009, 35, 727.
17 S. Feng, X. Chen, Y. Zhou, W. Tu, P. Li, H. Li, Z. Zou, Nanoscale, 2014, 6, 1896.
18 J. Wang, L. Qin, Y. Huang, P. Cai, H.-J. Seo, Mater. Lett., 2014, 125, 89.
19 Y. Guan, Y. Huang, T. Tsuboi, W. Huang, C. Chen, P. Cai, H.-J. Seo, Mater. Sci. Eng. B, 2014, 190, 26-32.
20 E.V. Murashov, Yu.A. Velikodnyi, V.D. Zhuravlev, Zhurnal Neorganicheskoi Khimii, 1993, 38, 1453.
21 H.M. Rietveld, J. Appl. Cryst., 1969,2, 65.
22 D. Balzar, in Microstructure Analysis from Diffraction (Eds.: R.L. Snyder, H.J. Bunge, J. Fiala), Oxford University Press/International Union of Crystallography, 1999.
23 a) R.W. Cheary, A.A. Coelho, J. Appl. Cryst., 1998,31, 851; b) R.W. Cheary, A.A. Coelho, J. Appl. Cryst., 1998, 3, 862.
24 a) K.H. Tytko, J. Mehmke, S. Fischer (1999) Structure and Bonding (Eds.: A.J.Bard, I.G. Dance,P. Day FRS, J.A. Ibers, T. Kunitake, T.J. Meyer, D.M.P. Mingos, H. W. Roesky, J.-P. Sauvage, A. Simon, F. Wudl) 93, 1-66;b) D. Brown, D.I. Altermatt, Acta Cryst., 1985, B41, 244.
25 N.V.Y. Scarlett, I.C. Madsen, Powder Diffraction, 2006, 21, 278.
26 a) B. Delley, J. Chem. Phys.,1990,92, 508; b) B. Delley, J. Chem. Phys. 2000, 113, 7756; c) B. Delley, Int. J. Quant. Chem., 1998, 69, 423.
27 J.P. Perdew, K. Burke, M. Ernzerhof, Phys. Rev. Lett., 1996, 77, 3865.
28 Yu. A. Velikodnyi, V.K. Trunov, O.V. Kudin, V.D. Zhuravlev, Kristallografiya, 1985, 30, 663.
29 E.V. Murashova, Yu.A. Velikodnyi, V.K. Trunov, Kristallografiya, 1991, 36, 617.
30 M. Neslpolo, G. Ferraris, H. Ohashi, Acta Cryst., 1999, B55, 902.

31 C. Muller, Hk. Muller-Buschbaum, J. Alloys Compd., 1993, 191, 251.
32 X. Wang, D.A. Vander Griend, Ch.L. Stern, K.R. Poeppelmeier, J. Alloys Compd., 2000, 298, 119.
33 T.-H. Noh, I.-S. Cho, S. Lee, D.-W. Kim, S. Park,S.-W.Seo, C.-W. Lee, K.-S. Hong, J. Am. Ceram. Soc., 2012, 95, 227.

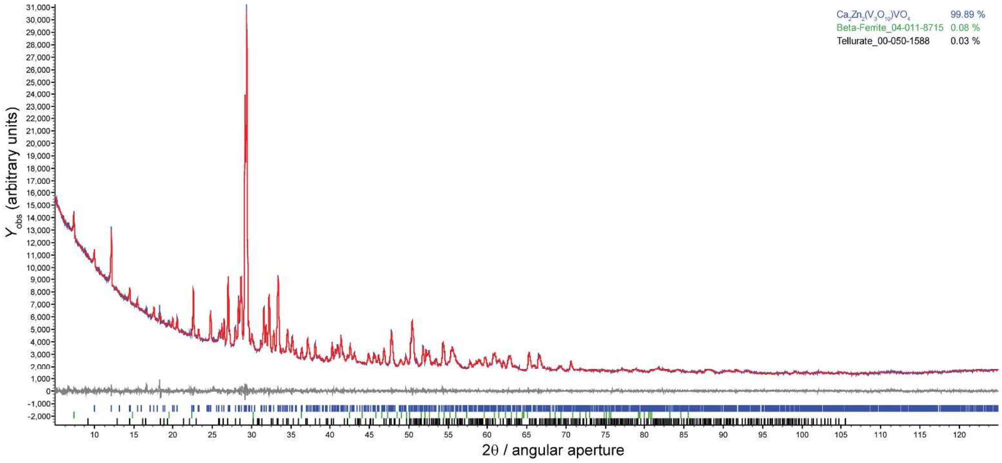
Ca2Zn2(V3O10)VO4 99.89 %
Beta-Ferrite_04-011-8715 0.08 %
Tellurate_00-050-1588 0.03 %
Yobs (arbitrary units)
31,000
30,000
29,000
28,000
27,000
26,000
25,000
24,000
23,000
22,000
21,000
20,000
19,000
18,000
17,000
16,000
15,000
14,000
13,000
12,000
11,000
10,000
9,000
8,000
7,000
6,000
5,000
4,000
3,000
2,000
1,000
0
-1,000
-2,000
10
15
20
25
30
35
40
45
50
55
60
65
70
75
80
85
90
95
100
105
110
115
120
2θ / angular aperture

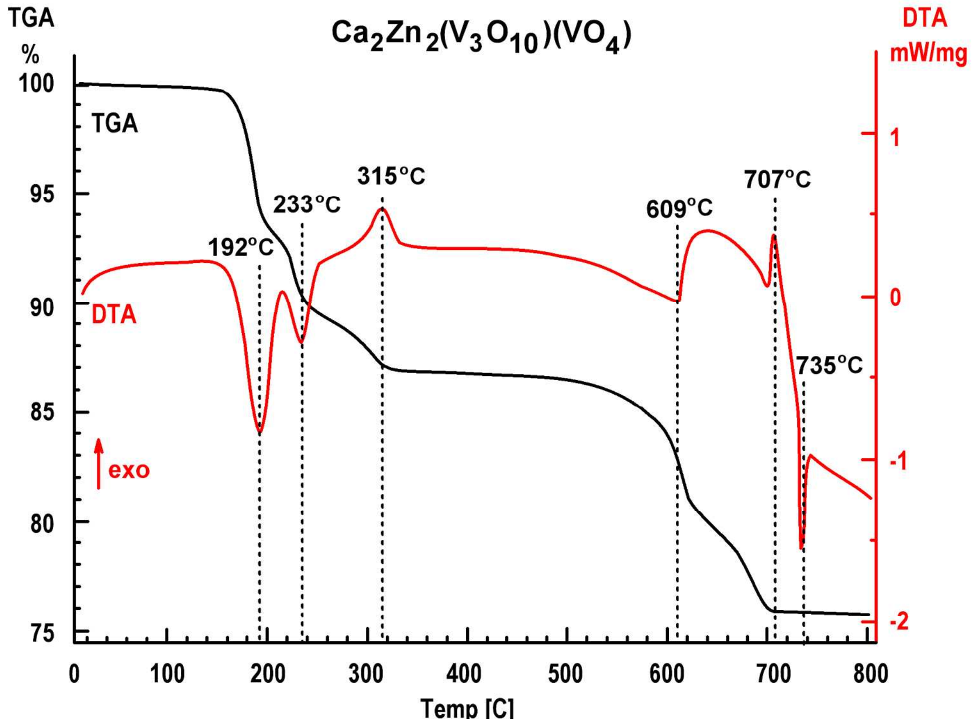
Ca2Zn2(V3O10)(VO4)
TGA
%
DTA
mW/mg
100
95
90
85
80
75
1
0
-1
-2
TGA
DTA
exo
192°C
233°C
315°C
609°C
707°C
735°C
0
100
200
300
400
500
600
700
800
Temp [C]

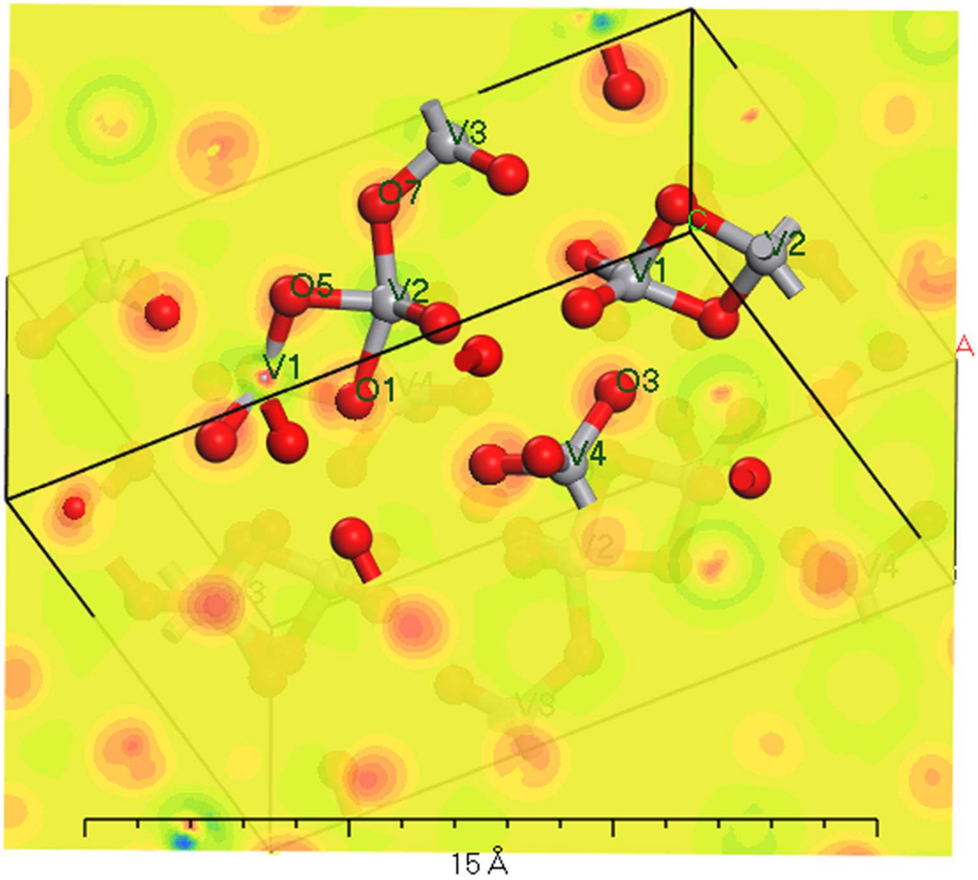
V3
O7
O5
V2
V1
O1
V1
V2
C
O3
V4
A
15 Å

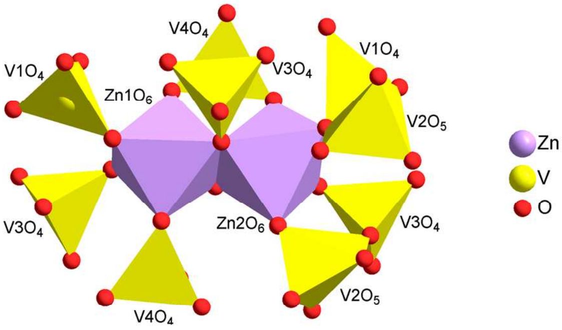
V4O$_4$
V1O$_4$
V3O$_4$
V1O$_4$
Zn1O$_6$
V2O$_5$
Zn
V
O
V3O$_4$
Zn2O$_6$
V3O$_4$
V2O$_5$
V4O$_4$

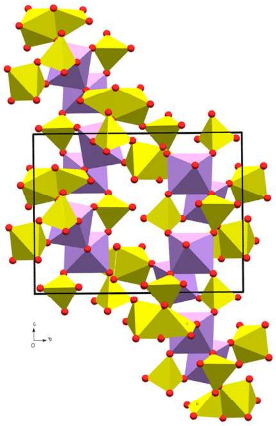

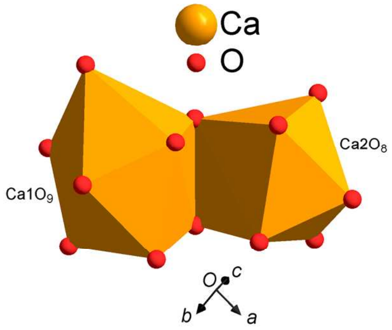
Ca
O
Ca2O$_8$
Ca1O$_9$
O
c
b
a

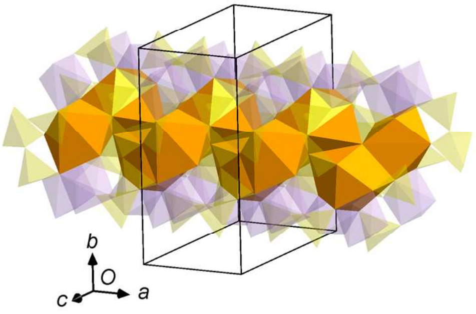
b
O
c
a

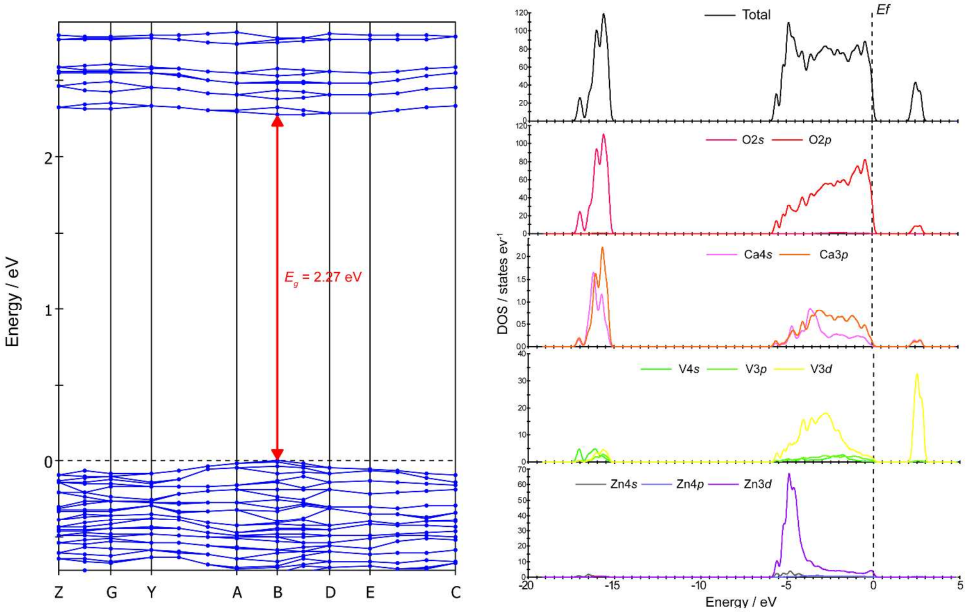
Energy / eV
0
1
2
$E_g$ = 2.27 eV
Z
G
Y
A
B
D
E
C
Total
Ef
O2s
O2p
Ca4s
Ca3p
V4s
V3p
V3d
Zn4s
Zn4p
Zn3d
DOS / states ev$^{-1}$
-20
-15
-10
-5
0
5
Energy / eV

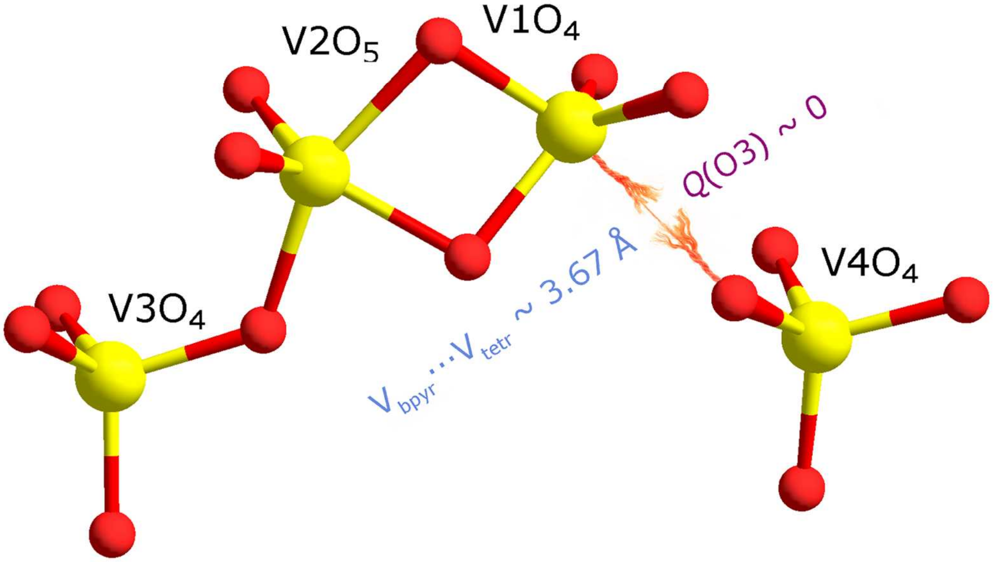
V2O5
V1O4
V3O4
V4O4
Q(O3) ~ 0
V bpyr···V tetr ~ 3.67 Å